Hydrogen-Nitrogen Greenhouse Warming in Earth's Early Atmosphere
Robin Wordsworth and Raymond Pierrehumbert
Science **339**, 64 (2013);
DOI: 10.1126/science.1225759

Hydrogen-Nitrogen Greenhouse Warming in Earth's Early Atmosphere

Robin Wordsworth* and Raymond Pierrehumbert

Understanding how Earth has sustained surface liquid water throughout its history remains a key challenge, given that the Sun's luminosity was much lower in the past. Here we show that with an atmospheric composition consistent with the most recent constraints, the early Earth would have been significantly warmed by H_2-N_2 collision–induced absorption. With two to three times the present-day atmospheric mass of N_2 and a H_2 mixing ratio of 0.1, H_2-N_2 warming would be sufficient to raise global mean surface temperatures above 0°C under 75% of present-day solar flux, with CO_2 levels only 2 to 25 times the present-day values. Depending on their time of emergence and diversification, early methanogens may have caused global cooling via the conversion of H_2 and CO_2 to CH_4, with potentially observable consequences in the geological record.

One of the most durable questions about Earth's early climate arises from the faint young Sun effect: Because progressive accumulation of He in a star's core causes its luminosity to increase with age (*1*), the solar energy incident on Earth was significantly lower [~75% of present-day values 3.8 billion years ago (Ga)] during the Hadean and Archean eras (*2*). Because geological evidence shows that Earth was not in a globally glaciated, snowball state throughout this time (*3*), additional mechanisms must have been present to warm the climate.

Previous explanations for this altered climate have included increased atmospheric ammonia or CH_4, a decreased surface albedo, and changes in the distribution of clouds (*2*, *4*, *5*). However, all of these mechanisms have subsequently been shown to suffer important defects (*6*, *7*). Increased atmospheric CO_2 is one plausible solution because of the climate buffer provided by the crustal carbonate-silicate cycle (*8*), but efficient mantle CO_2 cycling in the Hadean and Archean probably reduced the strength of this feedback (*9*). Interpretation of the geological record is difficult, but analyses of mid- to late Archean paleosols suggest between ~10 and 50 times the present atmospheric level (PAL) of CO_2 (*7*, *10*). Even lower values (around three times PAL) have been derived from analysis of magnetite and siderite equilibria in Archean banded iron formations, although the underlying assumptions behind these limits have been questioned (*5*, *7*).

One recently proposed mechanism for counteracting the faint young Sun is pressure-induced broadening of the absorption lines of existing greenhouse gases due to increased atmospheric N_2, which alone should cause a warming of between 3 and 8 K (*11*). Recent attempts to estimate atmospheric density from fossil raindrop imprints suggest a value near that of the present day around 2.7 Ga, with an upper limit of double the present value (*12*). However, the mantle has a large N inventory that is correlated with radiogenic ^{40}Ar but not primordial ^{36}Ar, indicating that it originated from subducted crust, where it had most likely been fixed biologically. It is therefore likely that on the pre-biotic/early Archean Earth, the atmospheric N_2 content was around two to three times the present-day value (*11*).

Hydrogen, the most abundant gas in the solar system, has previously been ignored in the Archean climate budget, presumably because it was long thought to be a minor constituent even in the early atmosphere (*13*). After the initial loss of Earth's primordial hydrogen envelope, the mixing ratio of H_2 in the atmosphere was primarily determined by a balance between outgassing, surface/ocean chemistry, and escape to space. It was long believed that the escape of H_2 in the Archean was rapid, with diffusion from the lower atmosphere to the exobase the limiting factor, as it is today. However, recent numerical calculations imply that the rate of hydrodynamic H_2 escape on the early Earth was more strongly constrained by the adiabatic cooling of the escaping gas, given a limited extreme ultraviolet (XUV) energy input (*14*–*16*). As a result, H_2 could have been a major constituent (up to ~30% by volume) of the Archean atmosphere unless surface or ocean biogeochemistry continuously removed it.

A single H_2 molecule is homonuclear and diatomic and hence has no direct vibrational or rotational absorption bands. Nonetheless, mo-

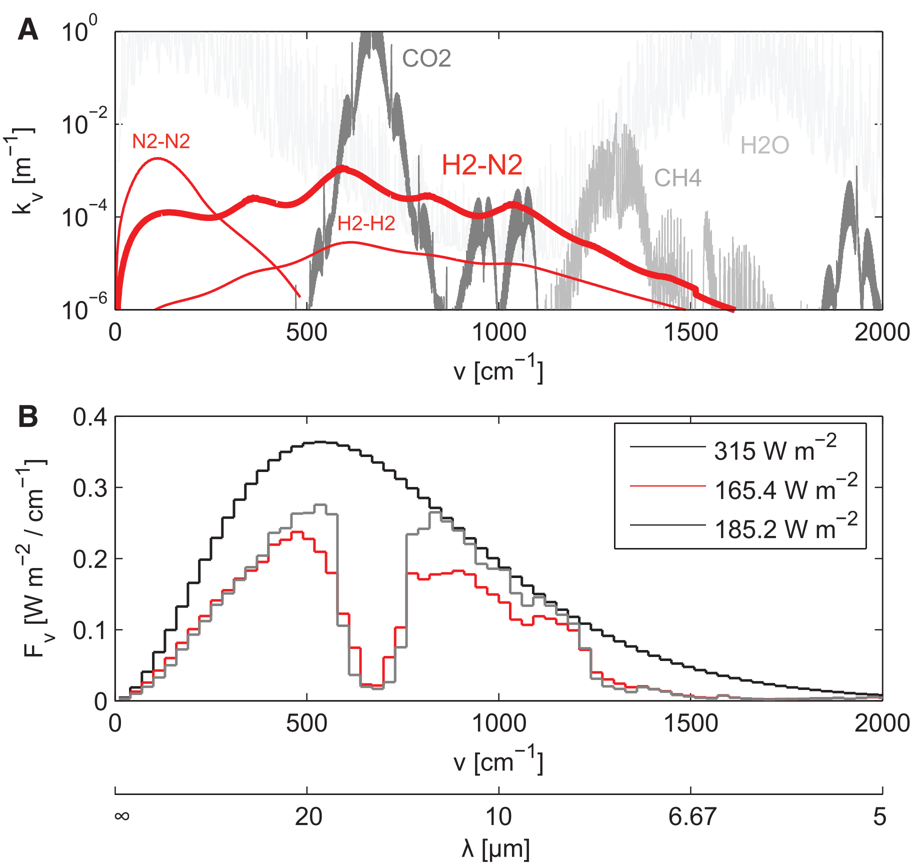

Fig. 1. (**A**) Infrared absorption at the surface for an Archean atmosphere with 3 × PAL N_2, 10% H_2, 1700 ppm CO_2 (~10 × PAL), 5 ppm CH_4, surface temperature 273 K, and relative humidity 0.77. k_v, absorptivity per unit of length; *v*, wavenumber. (**B**) Corresponding outgoing longwave radiation (OLR), assuming line absorption only (gray line) and with CIA included (red line). F_v, flux per unit wavenumber. The black line shows the blackbody emission at 273 K, and the numbers in the inset show the integrated OLR for each case. See the supplementary materials for calculation details. Given high atmospheric H_2 and N_2 levels, H_2-N_2 absorption dominates in the 750 to 1200 cm^{-1} spectral region, where the bands of the other greenhouse gases are relatively weak.

Department of Geological Sciences, University of Chicago, Chicago, IL 60637, USA.

*To whom correspondence should be addressed. E-mail: rwordsworth@uchicago.edu

lecular hydrogen interacts strongly with infrared radiation via collision-induced absorption (CIA), the strength of which scales with the product of the densities of the two interacting gases. CIA has been well studied for the gas giant planets and Titan, where it dominates radiative transfer in the middle and lower portions of the atmosphere (*17*, *18*). On early Earth, N_2 and H_2 may both have been abundant in the atmosphere, so interacting pairs of N_2-N_2, H_2-N_2, and H_2-H_2 should all be considered as potential contributors to greenhouse warming.

Figure 1A shows the H_2 and N_2 CIA bands alongside absorption bands of the other main greenhouse gases in the primitive atmosphere. Although N_2-N_2 dimer absorption is strong in the 0 to 300 cm^{-1} part of the spectrum, it is overwhelmed by H_2O absorption and is too far from the peak of blackbody emission at terrestrial temperatures to have a significant effect. H_2-H_2 absorbs over a much broader spectral range, but the dependence of CIA on the squared density of the gas means that even for the upper-limit estimates of H_2 mixing ratios, its overall effect is small. The N_2-H_2 band, however, absorbs strongly, and it peaks near the critical 750 to 1200 cm^{-1} window region, where the contribution of all the other gases to opacity is small.

To investigate the climatic effects of this previously neglected opacity, we performed one-dimensional (1D) radiative-convective simulations for a range of plausible Archean atmospheric compositions. We used a correlated-*k*, two-stream radiative transfer scheme (*19*) with 80 bands in the infrared and 36 bands in the visible. Temperature-pressure profiles were created over 80 vertical levels, with moist adiabatic adjustment assumed when the temperature profile became unstable to convection. A solar flux of 75% of the present-day level (1024.5 W m^{-2}) was assumed, and the surface albedo was set to 0.23 (*20*).

Figure 1B shows the resulting decrease in outgoing longwave radiation (OLR) in each band due to the presence of H_2 for an atmosphere with the same composition as shown in Fig. 1A. The OLR is significantly reduced in the 750 to 1200 cm^{-1} window region and around 500 cm^{-1}, whereas minor increases occur around the 15-µm CO_2 absorption band because of the decrease in atmospheric lapse rate as H_2 levels increase. Because the H_2-N_2 absorption spectrum overlaps with those of water vapor and CO_2, radiative forcing from H_2-N_2 is highest when these gases are scarce. The radiative forcing also increases strongly with the atmospheric N_2 content because of the dependence of CIA on the density of each interactant. At the PAL of N_2, H_2-N_2 CIA provides only a few watts per square meter, whereas for temperatures of 280 K or less in the "high" warming scenario with PAL CO_2, radiative forcing exceeds 24 W m^{-2} (Table 1 and Fig. 2B) (*21*).

To determine the increase in equilibrium surface temperature under this forcing, we next ran the radiative-convective model in time-stepping mode. Figure 2, C to E, shows that when atmospheric N_2 is elevated, higher H_2 mixing ratios cause significant increases in surface temperature. At PAL N_2, H_2-N_2 CIA causes at most 2 to 3 K of warming, but this rises to 10 to 15 K as N_2 levels are increased. Given a H_2 mixing ratio of 10% and 2 × PAL N_2, mean surface temperatures exceed the melting point of water for CO_2 levels ~25 × PAL. At 3 × PAL N_2, only ~2 × PAL CO_2 is required.

To what extent could H_2-N_2 warming have influenced the evolution of Earth's early climate? We can begin by considering the limiting case where no significant biological alteration of the atmosphere occurred. Then, the H_2 abundance in the early atmosphere can be determined by a

Table 1. Definitions of the atmospheric scenarios used in Figs. 2 and 3.

Scenario	N_2 mass column (kg m^{-2})	H_2 volume mixing ratio (mol/mol)
Present-day	7.80×10^3	0.0
Moderate	1.56×10^4	0.05
High	2.34×10^4	0.1

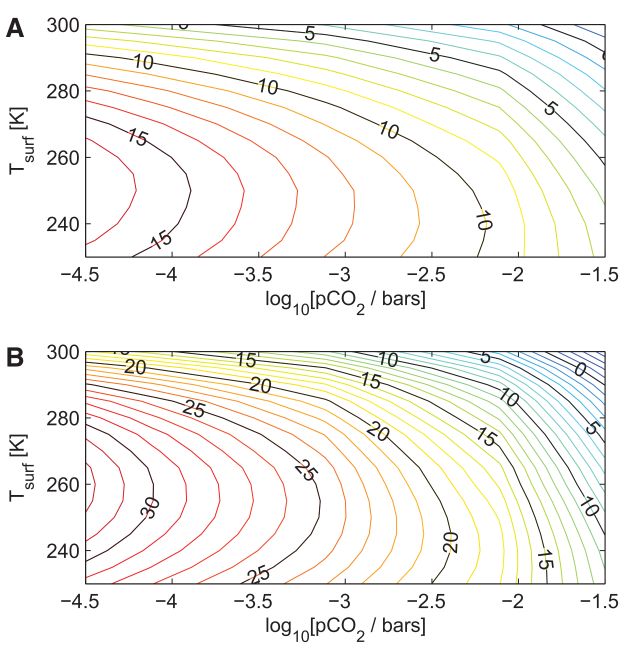

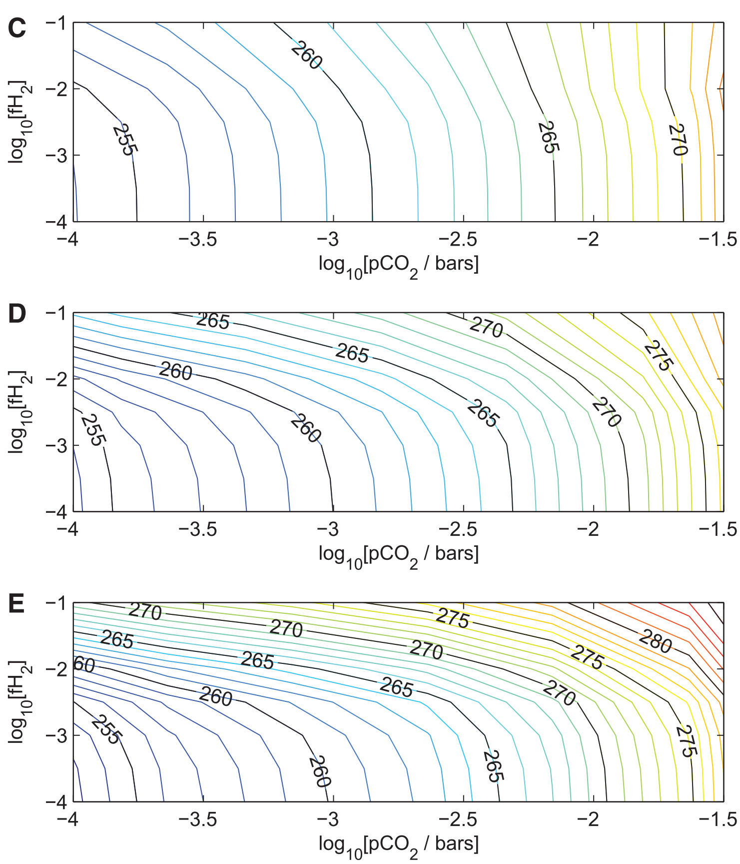

Fig. 2. Radiative forcing due to the presence of H for (**A**) moderate and (**B**) high H_2-N_2 warming scenarios (Table 1), as a function of surface temperature and atmospheric CO_2 partial pressure. The calculated surface temperature in thermal equilibrium as a function of atmospheric H_2 volume mixing ratio and CO_2 partial pressure, for a reduced solar flux F = 0.75 present-day solar flux (F_0) and total atmospheric N_2 amounts (**C**) one, (**D**) two, and (**E**) three times that of Earth today. Results are shown assuming no atmospheric CH_4 and a surface albedo of 0.23.

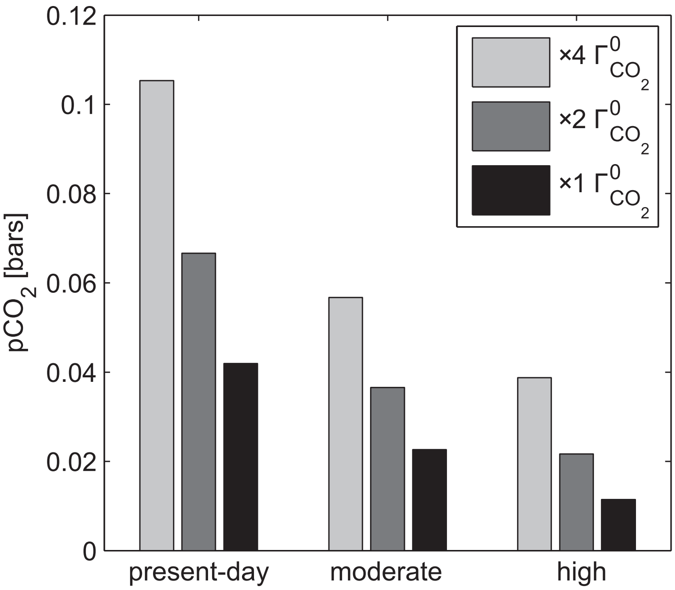

Fig. 3. Atmospheric CO_2 partial pressure, assuming an abiotic carbonate-silicate weathering feedback, no seafloor weathering, and a solar flux $F = 0.75\ F_0$. The H_2 and N_2 levels for the present-day, moderate, and high scenarios are given in Table 1. Results are shown for three values of the CO_2 outgassing rate Γ_{CO_2} as a function of the present-day rate.

simple balance between volcanic outgassing and escape to space, based on atmospheric redox balance in the absence of significant organic burial (*22*). Abiotic CO_2 levels can then be estimated by assuming that the carbonate-silicate temperature-weathering feedback (*8*) operated on 1- to 10-million-year time scales, driving atmospheric CO_2 downward to a level dependent on the solar flux and the amount of H_2 and N_2 in the atmosphere (*23*). Figure 3 shows estimated CO_2 concentrations under 75% of the present-day solar flux for various CO_2 outgassing rates, assuming no biological alteration of the atmosphere. Seafloor weathering is neglected in the calculation (*9*), so the CO_2 levels shown are most likely overestimated. Even so, it is clear that high H_2 and N_2 could easily have reduced atmospheric CO_2 to below 100 × PAL even under 75% solar flux.

After the emergence of life, the extent of biological alteration of the atmosphere was dependent on the energy source and net productivity of the dominant ecosystem. Of particular interest in the context of H_2-rich atmospheres are methanogens, which feed on the chemical energy released by combining CO_2 and H_2 in the reaction $CO_2 + 4H_2 \rightarrow CH_4 + 2H_2O$. Phylogenetic analyses suggest that these organisms evolved at some point in the mid-Archean, with hyperthermophilic methanogenesis preceding the mesophilic adaptation by at least several hundred million years (*24*, *25*). Although in small quantities CH_4 causes warming, its potential as a greenhouse gas is limited by the separation of its main absorption band from the peak of blackbody absorption (Fig. 1A) and its conversion to photochemical haze for $[CH_4]/[CO_2]$ ratios greater than ~0.1, which tends to have a cooling effect (*6*).

For methanogens to have increased surface temperatures after their emergence, therefore, the biological conversion of CO_2 and H_2 to CH_4 must have balanced CH_4 photolysis due to the solar UV flux at relatively low atmospheric CH_4 levels. Estimates of the CH_4 photolysis rate under the elevated UV/Lyman-α fluxes expected in the Archean are in the range 2×10^{11} to 5×10^{11} cm^{-2} s^{-1} for hydrogen-rich atmospheres (*26*). For comparison, the present-day biogenic CH_4 flux is on the order of 1×10^{11} cm^{-2} s^{-1} (*26*). Ecosystem models that assume no nutrient or climate constraints for biological productivity yield steady-state $[CH_4]/[H_2]$ ratios of around 0.03 if H_2 is initially abundant, implying an extremely hazy atmosphere and little warming from H_2-N_2 CIA (*26*). However, in the early Archean, the reduced continental area and increased ocean volume likely made nutrient and habitat limitations significantly more stringent than they are today (*27*).

If habitat limitations were not important, emergent methanogens in an early climate dominated by H_2-N_2 and CO_2 warming would have continued to consume H_2 and CO_2 rapidly until global cooling became the limiting factor on biological productivity (*28*). In the most drastic scenario, global glaciation would result, followed by a buildup of CO_2 and H_2 levels until the climate warmed again. Earth was ice-free throughout most of the Archean, but geological evidence exists for an early glaciation event 2.8 to 2.9 Ga (*29*), which may have been caused by the rise of methanogenesis. Understanding the detailed effects of the early biosphere on climate requires 3D climate simulations coupled with models of the (local) dependence of ecosystem productivity on surface temperature and nutrient availability. This is an important topic for future study.

Methanogens are often assumed to have been an integral part of the early Archean ecosystem because a CH_4 greenhouse was believed necessary to solve the faint young Sun problem. In contrast, our results show that an early climate dominated by abiotic H_2-N_2 and CO_2 warming is consistent with both observational and theoretical limits on atmospheric CO_2 levels and phylogenetic analyses suggesting later diversification of the Archaea. H_2-N_2 warming is also likely to be important in the search for biosignatures on super-Earth exoplanets, whose higher masses imply lower energy-limited hydrogen escape rates and larger typical atmospheric N_2 inventories. Because incident XUV flux is a function of orbital distance, H_2-N_2 warming may be of particular importance to the habitability of terrestrial exoplanets that are far from their host stars.

References and Notes

1. D. O. Gough, *Sol. Phys.* **74**, 21 (1981).
2. C. Sagan, G. Mullen, *Science* **177**, 52 (1972).
3. W. H. Peck, J. W. Valley, S. A. Wilde, C. M. Graham, *Geochim. Cosmochim. Acta* **65**, 4215 (2001).
4. A. A. Pavlov, L. L. Brown, J. F. Kasting, *J. Geophys. Res.* **106**, 23267 (2001).
5. M. T. Rosing, D. K. Bird, N. H. Sleep, C. J. Bjerrum, *Nature* **464**, 744 (2010).
6. J. D. Haqq-Misra, S. D. Domagal-Goldman, P. J. Kasting, J. F. Kasting, *Astrobiology* **8**, 1127 (2008).
7. G. Feulner, *Rev. Geophys.* **50**, RG2006 (2012).
8. J. C. G. Walker, P. B. Hays, J. F. Kasting, *J. Geophys. Res.* **86**, 9776 (1981).
9. N. H. Sleep, K. Zahnle, *J. Geophys. Res.* **106**, 1373 (2001).
10. S. G. Driese *et al.*, *Precambrian Res.* **189**, 1 (2011).
11. C. Goldblatt *et al.*, *Nat. Geosci.* **2**, 891 (2009).
12. S. M. Som, D. C. Catling, J. P. Harnmeijer, P. M. Polivka, R. Buick, *Nature* **484**, 359 (2012).
13. For exosolar planets, it has been suggested that H_2 could enable planetary habitability in certain cases, but only in quantities of 1 bar or more due to direct H_2-H_2 CIA (*30*–*32*). This mechanism was considered and dismissed for the early Earth in (*2*).
14. A. J. Watson, T. M. Donahue, J. C. G. Walker, *Icarus* **48**, 150 (1981).
15. F. Tian, O. B. Toon, A. A. Pavlov, H. De Sterck, *Science* **308**, 1014 (2005).
16. The calculations in (*15*) did not take nonthermal escape or heating due to heavier gases into account, leading to some claims that they underestimated the total H_2 escape (*33*). However, nonthermal escape is only dominant on the present-day Earth and should have been limited in the Archean (*34*), and infrared emission from radiatively active neutral species such as CO_2 causes significant cooling of the thermosphere. A final assessment of the hydrogen escape rates from Earth's early atmosphere awaits development of 3D multicomponent hydrodynamic escape models with coupled radiative transfer and chemistry.
17. A. Borysow, L. Frommhold, *Astrophys. J.* **303**, 495 (1986).
18. C. P. McKay, J. B. Pollack, R. Courtin, *Science* **253**, 1118 (1991).
19. R. Wordsworth *et al.*, *Astron. Astrophys.* **522**, A22+ (2010).
20. Materials and methods are available as supplementary materials on *Science* Online.
21. Here we use the term PAL to refer to present-day atmospheric partial pressure for CO_2 but present-day atmospheric mass for N_2. For all simulations, we first fix the mixing ratios of each gas and the total mass column of N_2, M_{N_2}. We then calculate the total atmospheric pressure as $p_{tot} = gM_{N_2}\overline{\mu}/\mu_{N_2}f_{N_2}$, where g is gravity, $\overline{\mu}$ is the mean molar mass, and f_{N_2} and μ_{N_2} are the volume mixing ratio and molar mass of N_2, respectively. The partial pressure of CO_2 is then simply $p_{tot}f_{CO_2}$.
22. J. F. Kasting, D. E. Canfield, *The Global Oxygen Cycle* (Wiley, Chichester, UK, 2012), pp. 93–104.
23. To produce Fig. 3 we expressed the CO_2 carbonate-silicate weathering rate as $\frac{W}{W_0} = \frac{\gamma}{\gamma_0}[1 + a_P(T_{surf} - T_0)]^a (\frac{p_{CO_2}}{p_{CO_2,0}})^b \exp(\frac{T_{surf} - T_0}{T_u})$ (*35*). We then set W equal to the assumed CO_2 outgassing rate

Γ_{CO_2} and calculated T_{surf} as a function of the CO_2 partial pressure p_{CO_2} using results from the radiative-convective model. See the supplementary materials for a definition of all terms and justification of the method.
24. C. H. House, B. Runnegar, S. T. Fitz-Gibbon, *Geobiology* **1**, 15 (2003).
25. C. E. Blank, *Geobiology* **7**, 495 (2009).
26. P. Kharecha, J. Kasting, J. Siefert, *Geobiology* **3**, 53 (2005).
27. Modern ocean net primary productivity is concentrated in shallow regions close to continents (*26*), but in the early Archean, the continental crust volume was about three times lower and the ocean volume may have been up to 25% greater than today (*36*, *37*). In the deep ocean away from submarine vents, rates of H_2 supply would be reduced by ~10^3 as compared to the mixed layer, implying a decrease of biological productivity there by a similar factor (*26*).
28. Indirectly, abundant methanogenesis could also have caused global cooling via drawdown of atmospheric N_2. In atmospheres with 1000 parts per million (ppm) CH_4, atmospheric HCN production rates via photolysis can reach 1×10^{10} cm^{-2} s^{-1} (*38*). Without a mechanism to reform N_2, this could cause the removal of the entire present-day atmospheric N_2 inventory on a time scale on the order of 100 million years.
29. G. M. Young, V. von Brunn, D. J. C. Gold, W. E. L. Minter, *J. Geol.* **106**, 523 (1998).
30. D. J. Stevenson, *Nature* **400**, 32 (1999).
31. R. Pierrehumbert, E. Gaidos, *The Astrophysical Journal Letters* **734**, L13 (2011).
32. R. Wordsworth, *Icarus* **219**, 267 (2012).
33. D. C. Catling, *Science* **311**, 38 (2006).
34. F. Tian, O. B. Toon, A. A. Pavlov, *Science* **311**, 38 (2006).
35. D. S. Abbot, N. B. Cowan, F. J. Ciesla, *Astrophys. J.* **178**, 756 (2012).
36. B. Dhuime, C. J. Hawkesworth, P. A. Cawood, C. D. Storey, *Science* **335**, 1334 (2012).
37. E. C. Pope, D. K. Bird, M. T. Rosing, *Proc. Natl. Acad. Sci. U.S.A.* **109**, 4371 (2012).
38. F. Tian, J. F. Kasting, K. Zahnle, *Earth Planet. Sci. Lett.* **308**, 417 (2011).

Acknowledgments: Climate calculations were performed on the iDataPlex computational cluster of the Université de Paris 6, France. R.W. thanks S. Lewis, J. Waldbauer, C. Goldblatt, N. Dauphas, M. Coleman, and D. Abbot for insightful discussions.

Supplementary Materials
www.sciencemag.org/cgi/content/full/339/6115/64/DC1
Materials and Methods
References

7 June 2012; accepted 5 November 2012
10.1126/science.1225759

Highly Variable El Niño–Southern Oscillation Throughout the Holocene

Kim M. Cobb,[1]* Niko Westphal,[2]† Hussein R. Sayani,[1] Jordan T. Watson,[2] Emanuele Di Lorenzo,[1] H. Cheng,[3,4] R. L. Edwards,[4] Christopher D. Charles[2]

The El Niño–Southern Oscillation (ENSO) drives large changes in global climate patterns from year to year, yet its sensitivity to continued anthropogenic greenhouse forcing is uncertain. We analyzed fossil coral reconstructions of ENSO spanning the past 7000 years from the Northern Line Islands, located in the center of action for ENSO. The corals document highly variable ENSO activity, with no evidence for a systematic trend in ENSO variance, which is contrary to some models that exhibit a response to insolation forcing over this same period. Twentieth-century ENSO variance is significantly higher than average fossil coral ENSO variance but is not unprecedented. Our results suggest that forced changes in ENSO, whether natural or anthropogenic, may be difficult to detect against a background of large internal variability.

The relative strength of the El Niño–Southern Oscillation (ENSO) phenomenon remains one of the most prominent uncertainties in general circulation model (GCM) projections of future climate change (*1*). ENSO is responsible for much of the interannual temperature and precipitation variability across the globe and thus influences energy and water use, ecosystem dynamics, and human health. Consequently, the broad range of ENSO projections represents a fundamental challenge for the development of meaningful climate change adaptation strategies. The uncertainty that arises from comparison of various models is compounded by the fact that instrumental records of ENSO are not sufficiently long to test the accuracy of any given model performance; these records are simply not long enough to provide robust estimates of natural ENSO variability.

[1]School of Earth and Atmospheric Sciences, Georgia Institute of Technology, Atlanta, GA 30332, USA. [2]Scripps Institution of Oceanography, La Jolla, CA 92037, USA. [3]Institute of Global Environmental Change, Xi'an Jiaotong University, Xi'an 710049, China. [4]Department of Earth Sciences, University of Minnesota, Minneapolis, MN 55455, USA.

*To whom correspondence should be addressed. E-mail: kcobb@eas.gatech.edu

†Present address: Department of Earth Sciences, Eidgenössische Technische Hochschule, CH-8092 Zürich, Switzerland.

Paleo-ENSO records can provide the necessary tests of GCM performance by tracking the response of ENSO to a variety of past natural climate forcings. One prominent example of this approach comes from the mid-Holocene [~6 thousand years (ky) ago] (*2*), an interval when both GCM simulations (*3*–*6*) and paleo-ENSO reconstructions (*7*–*10*) show reduced ENSO variability, associated with changes in insolation forcing (*11*). Such data-model agreement seemingly gives credence to the GCMs' abilities to simulate forced changes in ENSO. However, the paleoclimate evidence for a mid-Holocene reduction of ENSO variability is limited—it comprises millennia-long lake or marine sediment records that lack the resolution required to resolve ENSO explicitly (*8*–*10*), along with several fossil coral sequences that are seasonally resolved but short (*7*). Furthermore, the majority of these records rely on ENSO precipitation responses that may have changed through time.

We analyzed the ENSO variability contained in a collection of monthly resolved, uranium/thorium (U/Th)–dated fossil coral records spanning the past 7 ky from the central tropical Pacific. The archive roughly triples the amount of fossil coral data available to assess ENSO evolution through this time interval. The fossil corals come from Christmas (2°N, 157°W) and Fanning (4°N, 160°W) Islands, located in the Northern Line Islands, which are the site of numerous high-fidelity coral-based reconstructions of 20th-century ENSO spanning the past century (*12*–*14*) and millennium (*15*). These records allow for quantitative estimates of ENSO variance through time—estimates that can be used to gauge the magnitude of potential forced changes in ENSO variance, both natural and anthropogenic, with respect to natural ENSO variability. Such estimates of natural ENSO variability also provide particularly valuable tests of the long-term ENSO variability exhibited in millennia-long GCM simulations.

Previous work has demonstrated the accuracy and reproducibility of paleo-ENSO reconstructions constructed by using modern and fossil corals from Palmyra Island (6°N, 162°W), which is just north of Christmas and Fanning Islands (*15*). U/Th ages for the 17 fossil coral sequences (7 from Fanning and 10 from Christmas) presented in this study range from 1.3 to 6.9 ky (table S1). Scanning electron microscopy photos reveal evidence for extremely heterogeneous levels of diagenesis, with trace to moderate alteration (<5% by weight) sometimes visible in the same coral (fig. S1 and table S2). Like the modern corals, the fossil coral cores were processed following standard procedures and sampled at 1-mm intervals for oxygen isotopic ($\delta^{18}O$) analyses [long-term reproducibility of $\delta^{18}O$ is ± 0.07 per mil (1σ)] (*16*). The fossil corals' growth rates range from 8 to 20 mm/year, and the records range in length from 19 to 81 years (fig. S2 and table S2).

Northern Line Island coral $\delta^{18}O$ records reflect changes in sea-surface temperature (SST) as well as the $\delta^{18}O$ of seawater (the latter linearly correlated to sea-surface salinity) (*17*), both of which change during ENSO extremes. El Niño events bring warmer and rainier conditions to the Northern Line Islands, conditions which constructively act to decrease coral $\delta^{18}O$ (*12*–*14*). The opposite climatic effects occur during cool La Niña extremes, driving an increase in coral $\delta^{18}O$. Modern Line Islands coral $\delta^{18}O$ records are highly correlated to the regional-scale NIÑO3.4 index (defined as the average of instrumental SSTs from 5°S to 5°N, and from 120° to 170°W) (Fig. 1). As